Dose-dependent role of the cohesin complex in normal and malignant hematopoiesis

Aaron D. Viny,[1,2*] Christopher J. Ott,[6,7*] Barbara Spitzer,[1] Martin Rivas,[8] Cem Meydan,[8] Efthymia Papalexi,[1] Dana Yelin,[1,9] Kaitlyn Shank,[1] Jaime Reyes,[6] April Chiu,[3] Yevgeniy Romin,[4] Vitaly Boyko,[4] Swapna Thota,[10] Jaroslaw P. Maciejewski,[10] Ari Melnick,[8] James E. Bradner,[6,7**] and Ross L. Levine[1,2,5**]

[1]Human Oncology and Pathogenesis Program, [2]Leukemia Service, Department of Medicine, [3]Department of Pathology, [4]Molecular Cytology Core Facility, and [5]Center for Epigenetics Research, Memorial Sloan Kettering Cancer Center, New York, NY 10065
[6]Department of Medical Oncology, Dana-Farber Cancer Institute, Boston, MA 02215
[7]Department of Medicine, Harvard Medical School, Boston, MA 02115
[8]Department of Medicine, Weill Cornell Medical College, New York, NY 10065
[9]Department of Medicine, Rabin Medical Center, Beilinson Campus, Petah Tikvah 49100, Israel
[10]Department of Translational Hematology and Oncology Research, Taussig Cancer Institute, Cleveland Clinic, Cleveland, OH 44195

Cohesin complex members have recently been identified as putative tumor suppressors in hematologic and epithelial malignancies. The cohesin complex guides chromosome segregation; however, cohesin mutant leukemias do not show genomic instability. We hypothesized that reduced cohesin function alters chromatin structure and disrupts cis-regulatory architecture of hematopoietic progenitors. We investigated the consequences of *Smc3* deletion in normal and malignant hematopoiesis. Biallelic *Smc3* loss induced bone marrow aplasia with premature sister chromatid separation and revealed an absolute requirement for cohesin in hematopoietic stem cell (HSC) function. In contrast, *Smc3* haploinsufficiency increased self-renewal in vitro and in vivo, including competitive transplantation. *Smc3* haploinsufficiency reduced coordinated transcriptional output, including reduced expression of transcription factors and other genes associated with lineage commitment. *Smc3* haploinsufficiency cooperated with Flt3-ITD to induce acute leukemia in vivo, with potentiated Stat5 signaling and altered nucleolar topology. These data establish a dose dependency for cohesin in regulating chromatin structure and HSC function.

CORRESPONDENCE
Ross L. Levine:
leviner@mskcc.org
OR
James E. Bradner:
james_bradner@dfci.harvard.edu

Abbreviations used: AML, acute myeloid leukemia; GMP, granulocyte-macrophage progenitor; GSEA, gene set enrichment analysis; HSC, hematopoietic stem cell; HSPC, hematopoietic stem/progenitor cell; LT-HSC, long-term HSC; MDS, myelodysplastic syndrome; MEP, megakaryocyte-erythrocyte progenitor; MP, myeloid progenitor; MPP, multipotent progenitor; PIpC, polyinosinic:polycytidylic acid; qRT-PCR, quantitative real-time PCR; ST-HSC, short-term HSC; THS, transposase hypersensitive site; TSS, transcriptional start site.

Normal hematopoiesis is orchestrated by master regulatory transcription factors that are expressed in specific cell types at discrete differentiation stages (Novershtern et al., 2011; Lara-Astiaso et al., 2014). Tight coordination of these networks maintains the balance between hematopoietic stem/progenitor cell (HSPC) self-renewal and lineage commitment. In contrast, acute leukemias are characterized by increased self-renewal and impaired differentiation, often in the setting of mutations in genes with a known or postulated role in regulating transcriptional output (Dawson et al., 2012). Recent cancer genome sequencing studies have identified loss of function mutations in cohesin complex factors among patients with solid tumors (Solomon et al., 2011; Balbás-Martínez et al., 2013) and with myeloid malignancies (Jan et al., 2012; Welch et al., 2012; Cancer Genome Atlas Research Network, 2013; Kon et al., 2013; Thol et al., 2014; Thota et al., 2014), suggesting a role for cohesin as a tumor suppressor.

Cohesin is a multiprotein ring-like complex known to regulate sister chromatid alignment during mitosis; thus, it has been suggested that cohesin mutations will induce chromosomal instability (Solomon et al., 2011). However, cohesin mutations are not associated with aneuploidy, suggesting an alternate pathophysiologic mechanism (Thota et al., 2014). Recent research has

*A.D. Viny and C.J. Ott contributed equally to this paper.
**J.E. Bradner and R.L. Levine contributed equally to this paper.

The Rockefeller University Press $30.00
J. Exp. Med. 2015 Vol. 212 No. 11 1819–1832
www.jem.org/cgi/doi/10.1084/jem.20151317

suggested a role for cohesin in regulation of gene expression by stabilizing interactions between promoters and distal cis-regulatory elements (or enhancers). This research suggests cohesin functions as an insulator factor, protecting promoters from distal enhancers, thus establishing boundaries around actively transcribed chromatin domains (Bell et al., 1999; Kagey et al., 2010; Merkenschlager and Odom, 2013). These activities are often in direct physical association with the DNA-binding factor CTCF (CCCTC-binding factor; Parelho et al., 2008; Rubio et al., 2008; Stedman et al., 2008; Wendt et al., 2008), although cohesin can also form promoter–enhancer and enhancer–enhancer loops in a CTCF-independent manner (Dowen et al., 2014). The formation of specific chromatin architecture through cohesin-mediated looping mediates the recruitment and activity of RNA polymerase II, facilitating transcriptional activation (Schaaf et al., 2013).

Genomic data strongly suggest cohesin complex members function as tumor suppressors, but the underlying mechanism by which these mutations disrupt hematopoiesis and promote transformation has not been delineated. Of note, myeloid malignancies such as myelodysplastic syndrome (MDS) and acute myelogenous leukemia (AML) with cohesin mutations are characterized by monoallelic mutations in any one of the cohesin complex members and never by complete loss of a cohesin complex member or by multiple heterozygous mutations. These data suggest a dose response for cohesin function in hematopoiesis, with heterozygous loss of a single cohesin complex member sufficient to contribute to leukemic transformation. We therefore sought to investigate the impact of complete loss of a specific cohesin subunit, *Smc3*, compared with *Smc3* haploinsufficiency on HSPC function in vivo.

RESULTS AND DISCUSSION

Development of a conditional *Smc3* allele

To delineate the role of Smc3 in hematopoietic function, we generated a conditional allele targeting *Smc3* in vivo. We used embryonic stem cells in which two LoxP sites were inserted flanking exon 4, a critical coil-coil domain, as well as Frt sites surrounding a neomycin cassette in an upstream intron (Fig. 1 A). After Frt-mediated excision of the neo cassette, mice were then crossed to the inducible cre-recombinase, Mx1. *Smc3* deletion was achieved after treatment with the IFN-α–stimulating polyinosinic:polycytidylic acid (PIpC).

Smc3 is required for hematopoietic stem cell (HSC) function and for normal hematopoiesis

We characterized the effects of homozygous *Smc3* loss by crossing mice bearing floxed alleles to Mx1-cre mice. Mice were treated with PIpC at 4 wk of age, resulting in complete recombination in Mx1-cre $Smc3^{fl/fl}$ mice (Fig. 1 B). We observed severe pancytopenia with decreased WBC ($P < 0.001$), decreased hemoglobin ($P < 0.001$), and decreased platelet count ($P < 0.001$) compared with littermate cre-negative controls (Fig. 1 C). Moreover, *Smc3* deletion in the hematopoietic compartment ($Smc3^{\Delta/\Delta}$) resulted in 100% lethality with a median survival of 11.5 d from the start of PIpC ($P < 0.001$; Fig. 1 D). At time of death, we observed evidence of cerebral hemorrhage in coronal brain sections and local tissue necrosis in spleen and liver tissue. Pathological analysis of femurs from *Smc3* KO mice revealed marked hypocellularity, and nucleolar staining of aspirates taken on day 5 after PIpC revealed increased numbers of discrete nucleoli (green) per cell with the TOTAL-NUCLEAR-ID red/green nucleolar/nuclear immunofluorescent staining kit on confocal microscopy (Fig. 1, E and F). Flow cytometry of peripheral blood at euthanasia revealed an absence of myeloid elements in $Smc3^{\Delta/\Delta}$ mice, with T lymphocytes ($Mac1^- Gr1^- Cd3^+ B220^-$) as the only remaining circulating WBCs (Fig. 1 G). These remaining cells did not show recombined floxed alleles and expressed Smc3 protein (not depicted). Chromosome morphology was difficult to assess, and we observed premature sister chromatid separation and tetraploidy/polyploidy in 44/200 (22%) of scored metaphases in *Smc3* KO mice (Fig. 1 H) compared with normal metaphase cytogenetics and sister chromatid separation in cre-negative littermate controls (not depicted). To assess the effects of *Smc3* deletion on HSC function in vivo, 500,000 BM cells from 6-wk-old Cd45.2 Mx1-cre $Smc3^{fl/fl}$ mice or cre-negative $Smc3^{fl/fl}$ littermate controls were transplanted with an equal number of 6-wk-old Cd45.1 competitor BM cells into lethally irradiated Cd45.1 recipient mice. Mice were treated with PIpC after engraftment. After PIpC-mediated deletion, *Smc3* KO cells showed complete loss of HSC function, as KO cells were completely outcompeted by WT BM in vivo (Fig. 1, I and J).

Impact of *Smc3* haploinsufficiency on hematopoiesis in vitro and in vivo

Mx1-cre mice bearing one floxed allele were treated with PIpC at 4 wk of age, resulting in one recombined allele and one WT allele (Fig. 1 B). We observed reduced Smc3 protein expression and we observed a 50% reduction in *Smc3* mRNA expression (Fig. 2, A and B). In methylcellulose plating assays (rmIL-3, rmSCF, rh-EPO, and eh-IL6), $Smc3^{\Delta/+}$ cells showed increased serial replating capacity, whereas cells derived from $Smc3^{fl/+}$ mice failed to replate after the third plating. Cells taken from the fourth plating continued to express a single *Smc3* allele (Fig. 2, B and C). 4 wk after PIpC treatment, we observed an increase in the absolute number of immunophenotypically defined HSPCs in $Smc3^{\Delta/+}$ mice, with a significant increase in absolute number of LSK ($Lin^- Sca\text{-}1^+ c\text{-}Kit^+$; $P = 0.005$) but a decrease in myeloid progenitor (MP) cells ($Lin^- Sca\text{-}1^- c\text{-}Kit^+$; $P = 0.003$; Fig. 2, D and G). Within the LSK compartment, we observed an increase in short-term HSCs (ST-HSCs; $Cd150^+ Cd48^+ Lin^- Sca\text{-}1^+ c\text{-}Kit^+$; $P = 0.008$), a significant decrease in the frequency of long-term HSCs (LT-HSCs; $Cd150^+ Cd48^- Lin^- Sca\text{-}1^+ c\text{-}Kit^+$; $P < 0.001$) and a significant increase in the absolute number of multipotent progenitor (MPP) populations ($Cd150^- Cd48^+ Lin^- Sca\text{-}1^+ c\text{-}Kit^+$; $P = 0.003$; Fig. 2 E). No differences were seen within the MP populations (Fig. 2 F). Nucleolar staining

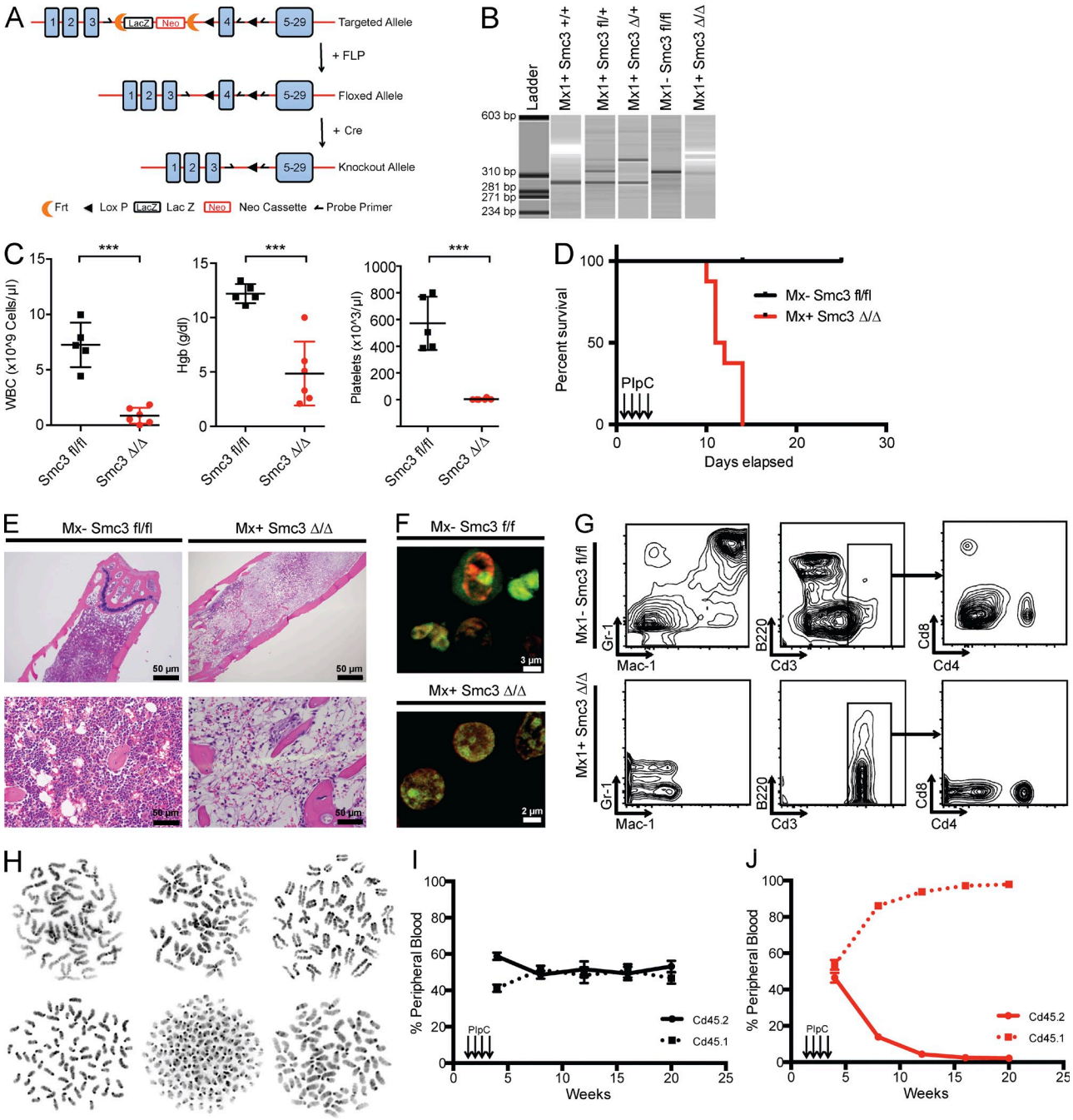

Figure 1. ***Smc3* is required for HSC function.** (A) Schematic depiction of the targeted *Smc3* allele. Exon 4 is targeted and flanked by LoxP sites upon Frt-mediated deletion of the Neo cassette. (B) Qiaxel gel electrophoresis image of PCR genotyping of the *Smc3* WT allele (287 bp), *Smc3* floxed allele (313 bp), and Cre recombination allele (349 bp). The genotype is shown for $Smc3^{+/+}$, $Smc3^{fl/+}$, $Smc3^{\Delta/+}$, $Smc3^{fl/fl}$, and $Smc3^{\Delta/\Delta}$. (C) Peripheral blood WBCs, hemoglobin (Hgb), and platelets after postnatal deletion of *Smc3*. Counts are compared with age-matched controls injected with PIpC ($n = 6$ for each genotype). (D) Kaplan-Meier curve of primary mice after postnatal *Smc3* deletion ($n = 10$ for each genotype). (E) Histological (H&E) analysis of Mx1-Cre $Smc3^{\Delta/\Delta}$ and Cre-negative $Smc3^{fl/fl}$ control BM. (F) Nucleolar stain of Mx1-Cre $Smc3^{\Delta/\Delta}$ BM reveals fragmented and supernumerary nucleoli. ACK-lysed BM was stained with TOTAL-NUCLEAR-ID fluorescent reagents, allowing simultaneous staining of both the nucleoli (green) and total nucleus (red). (G) Flow cytometric enumeration of $B220^+$, $Cd11b^+/Gr1^+$, $Cd3^+$, and Cd4/8 ratio of cells in the peripheral blood of Mx1-Cre $Smc3^{fl/fl}$ mice and cre-negative controls. (H) Metaphase karyotyping upon exposure to colcemid (45 min): Representative metaphases with partial or complete premature sister chromatid separation resulting in tetraploidy/polyploidy in 44/200 cells (22%). (I and J) Competitive transplantation of 500K donor-derived Cd45.1 whole BM was injected by tail vein after lethal irradiation with either 500K Cd45.2 whole BM from Mx^- $Smc3^{fl/fl}$ or 500K Mx^+ $Smc3^{\Delta/\Delta}$ ($n = 5$ mice each genotype). Mice were treated with PIpC at week 2, and chimerism was measured by percentage of Cd45.2 in the peripheral blood every 4 wk. Error bars represent ± SD (C, I, and J); ***, $P < 0.001$ (Mann–Whitney U test).

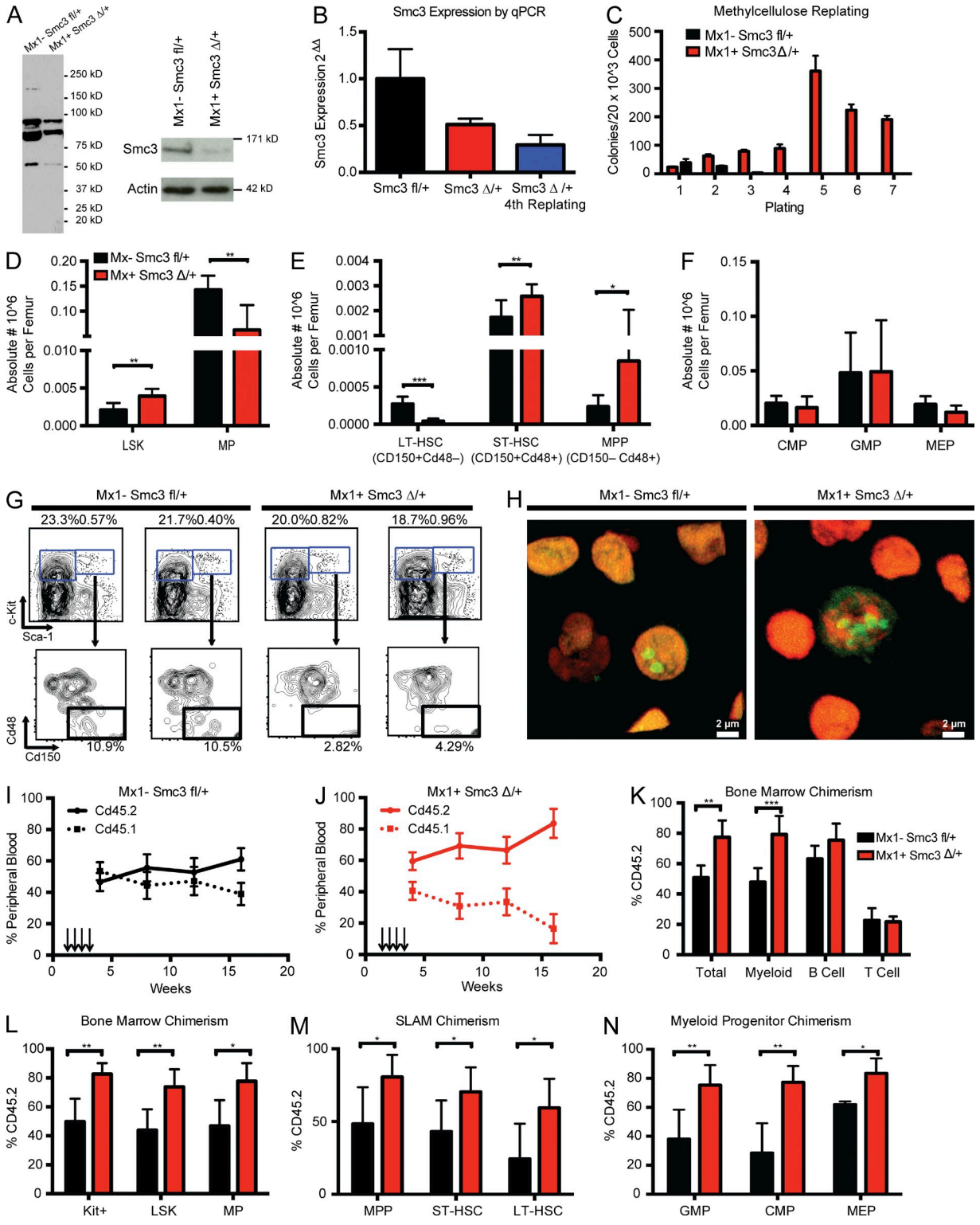

Figure 2. Smc3 haploinsufficiency increases stem cell self-renewal. (A) Mx1-cre–mediated deletion of *Smc3* confirmed by Western blot of BM. (B) qRT-PCR showing relative expression level of *Smc3* in BM and persistence of the decreased expression in the cells that replate in methylcellulose. (C) Serial plating and colony counts in methylcellulose for $Smc3^{fl/+}$ or $Smc3^{\Delta/+}$ BM. Whole BM was plated in triplicate at 20K cells/well. (D–F) Flow cytometric enumeration of BM c-Kit$^+$, LSK (Lin$^-$ Sca1$^+$ Kit$^+$), and MP (Lin$^-$ Sca1$^-$ Kit$^+$) cells (D), LT-HSCs (LSK CD150$^+$ CD48$^-$), ST-HSCs (LSK, Cd150$^+$, Cd48$^+$), and MPP cells (LSK CD150$^-$ CD48$^+$; E), and percentage of common myeloid progenitors (CMPs; lineage$^-$, c-Kit$^+$, Sca-1$^-$, FcγR$^-$, CD34$^+$), GMPs (lineage$^-$ c-Kit$^+$ Sca-1$^-$, FcγR$^+$ CD34$^+$), and MEPs (lineage$^-$ c-Kit$^+$ Sca-1$^-$ FcγR$^-$ CD34$^-$; F) in $Smc3^{fl/+}$ and $Smc3^{\Delta/+}$ mice (n = 4–6 mice per genotype). Mice were taken down at 4 wk after PIpC injection. Excision was confirmed at takedown. Data are expressed as frequency of live cells per femur. (G) Representative

revealed increased numbers of discrete nucleoli on confocal microscopy in *Smc3*$^{\Delta/+}$ BM, whereas cre-negative *Smc3*$^{fl/+}$ BM had singlet or doublet nucleoli exclusively (Fig. 2 H).

Smc3 haploinsufficiency increases self-renewal in vivo

To assess the effects of *Smc3* haploinsufficiency in vivo, 500,000 BM cells from 6-wk-old Cd45.2 Mx1-cre *Smc3*$^{fl/+}$ mice or cre-negative *Smc3*$^{fl/+}$ littermate controls were transplanted in competition with an equal number of 6-wk-old Cd45.1 competitor BM cells into lethally irradiated Cd45.1 recipient mice. Mice were treated with PIpC after engraftment 2 wk later. In contrast to the competitive disadvantage seen with *Smc3* KO BM in transplant assays, *Smc3* haploinsufficient BM outcompeted WT BM, consistent with increased self-renewal in vivo (Fig. 2, I and J). We observed increased chimerism in total BM ($P = 0.001$) and in the myeloid ($P = 0.002$) compartment with a trend toward increased chimerism in B lymphocytes ($P = 0.08$) but not in T lymphocytes ($P = 0.81$; Fig. 2 K). The increase in self-renewal observed in the competitive transplant assays was seen in all HSPC compartments (Fig. 2, L–N).

Heterozygous *Smc3* loss cooperates with *Flt3*-ITD to induce AML

AML patients with cohesin mutations often have concurrent FLT3-ITD mutations (Cancer Genome Atlas Research Network, 2013). We therefore investigated the phenotype of mice with concurrent *Smc3* haploinsufficiency and expression of the *Flt3*^{ITD} allele from the endogenous locus, compared with mice with *Flt3*^{ITD} alone (Lee et al., 2007). Whole BM from primary Mx1-cre *Smc3*$^{fl/+}$, cre-negative *Smc3*$^{fl/+}$ littermate control, Mx1-cre *Flt3*^{ITD}, and Mx1-cre *Smc3*$^{fl/+}$ *Flt3*^{ITD} was injected into lethally irradiated recipients along with support control marrow. Mice were PIpC injected after 2 wk and followed longitudinally. All Mx1-cre *Smc3*$^{\Delta/+}$ *Flt3*^{ITD} died of acute leukemia (median survival 167 d; $P < 0.001$), whereas there were no deaths in the Mx1-cre *Smc3*$^{\Delta/+}$, cre-negative *Smc3*$^{fl/+}$, or Mx1-cre *Flt3*^{ITD} cohorts ($P = 0.05$; Fig. 3 A). Serial transplantation of whole BM from leukemic Mx1-cre *Smc3*$^{\Delta/+}$ *Flt3*^{ITD} mice resulted in further anticipation of the leukemic disease with shortened disease latency (Fig. 3 B). All recipients developed AML hallmarked by leukocytosis, anemia, and thrombocytopenia (Fig. 3 C). Protein lysates from all four genotypes revealed decreased Smc3 expression in *Smc3* haploinsufficient and Mx1-cre *Smc3*$^{\Delta/+}$ *Flt3*^{ITD} BM without loss of the remaining *Smc3* allele or complete loss of Smc3 protein expression (Fig. 3 D). We noted splenomegaly in both *Flt3*^{ITD} and *Smc3*$^{fl/+}$ *Flt3*^{ITD} mice ($P = 0.03$; Fig. 3 E). Cytospins revealed that Mx1-cre *Smc3*$^{\Delta/+}$ *Flt3*^{ITD} mice were characterized by expansion of blasts in the blood and BM, with several discrete nucleoli in each blast. Blasts were evident throughout the marrow and spleen with marked dysmyelopoiesis, increased nucleoli, and dysplastic, hypolobated megakaryocytes (Fig. 3, F and G). We observed splenomegaly and a leukemoid appearance of the bones consistent with the increased number of stem and progenitor cells, and cytogenetic analysis revealed normal metaphase cytogenetics in all mice (not depicted). Although Mx1-cre *Flt3*^{ITD} stem and progenitor cells had singlet or doublet nucleoli, nearly every cell from the BM of Mx1-cre *Smc3*$^{\Delta/+}$ *Flt3*^{ITD} had three or more nucleoli (Fig. 3 G and Videos 1 and 2). Consistent with the morphological alterations observed in our mouse model, pathological analysis of a patient sample with concurrent SMC3 R288fs and FLT3-ITD mutations revealed an increase in nucleolar frequency in the blast population (Fig. 3 I). Mx1-cre *Smc3*$^{\Delta/+}$ *Flt3*^{ITD} BM cells showed increased serial replating, similar to the phenotype observed with *Smc3* haploinsufficiency but with higher numbers of colonies per plating (Fig. 3 J).

Alterations in the stem/progenitor compartment induced by concomitant *Smc3* heterozygous loss and expression of *Flt3*-ITD

We next assessed the effects of *Smc3* loss in concert with *Flt3*-ITD in the HSC and progenitor populations. We observed a significant increase in the absolute number of LSK cell (Lin$^-$ Sca-1$^+$ c-Kit$^+$) Mx1-cre *Smc3*$^{\Delta/+}$ *Flt3*^{ITD} mice compared with control ($P = 0.003$) and compared with Mx1-cre *Flt3*^{ITD} ($P = 0.008$; Fig. 3 K). Mx1-cre *Flt3*^{ITD} mice were characterized by an increase in MPs ($P = 0.018$) and granulocyte-macrophage progenitors (GMPs; lineage$^-$ c-Kit$^+$ Sca-1$^-$, FcγR$^+$ CD34$^+$; $P = 0.05$) compared with control, as previously reported (Lee et al., 2007; Shih et al., 2015). In contrast, concomitant *Smc3* haploinsufficiency in the setting of the *Flt3*^{ITD} significantly reduced the number of GMPs ($P = 0.04$; Fig. 3 L). The overall increase in the LSK population seen in Mx1-cre *Smc3*$^{\Delta/+}$ *Flt3*^{ITD} mice was driven mostly by an overall increase in the absolute number of ST-HSCs ($P = 0.005$ and 0.008 compared with *Smc3* and *Flt3* single mutations, respectively; Fig. 3 M), with a statistically significant decrease in LT-HSCs compared with both cre-negative *Smc3*$^{fl/+}$ and Mx1-cre *Flt3*^{ITD} ($P = 0.002$ and 0.001, respectively; Fig. 3 N) and an increase in MPPs (Lin$^-$ Sca-1$^+$ c-Kit$^+$ Cd48$^+$ Cd150$^-$; $P = 0.047$; Fig. 3 O).

FACS analysis of BM stem cell populations of *Smc3*$^{fl/+}$ and *Smc3*$^{\Delta/+}$ mice. (H) Nucleolar staining of *Smc3*$^{fl/+}$ and *Smc3*$^{\Delta/+}$ BM reveals occasional cells with supernumerary nucleoli in *Smc3*$^{\Delta/+}$ cells. (I and J) Competitive transplantation of 500K donor-derived Cd45.1 whole BM was injected by tail vein after lethal irradiation with either 500K Cd45.2 whole BM from *Smc3*$^{fl/+}$ or 500K *Smc3*$^{\Delta/+}$. Chimerism was measure by percentage of Cd45.2 in the peripheral blood every 4 wk. Mice were sacrificed at 20 wk. (K–N) Flow cytometric chimerism of unsorted peripheral blood, Mac1$^+$Gr1$^+$ myeloid cells, B220$^+$ B cells, and Cd3$^+$ T cells (K), BM c-Kit$^+$, LSK (Lin$^-$ Sca1$^+$ Kit$^+$), and MP (Lin$^-$ Sca1$^-$ Kit$^+$) cells (L), LT-HSCs (LSK CD150$^+$ CD48$^-$), ST-HSCs (LSK, Cd150$^+$, Cd48$^+$), and MPP cells (LSK CD150$^-$ CD48$^+$; M), and percentage of CMPs (lineage$^-$, c-Kit$^+$, Sca-1$^-$, FcγR$^-$, CD34$^+$), GMPs (lineage$^-$ c-Kit$^+$ Sca-1$^-$, FcγR$^+$ CD34$^+$), and MEPs (lineage$^-$ c-Kit$^+$ Sca-1$^-$ FcγR$^-$ CD34$^-$; N) in *Smc3*$^{fl/+}$ and *Smc3*$^{\Delta/+}$ mice ($n = 5$ mice per genotype). Error bars represent ± SD (B–F and I–N); *, $P < 0.05$; **, $P < 0.01$; ***, $P < 0.001$ (Mann–Whitney U test).

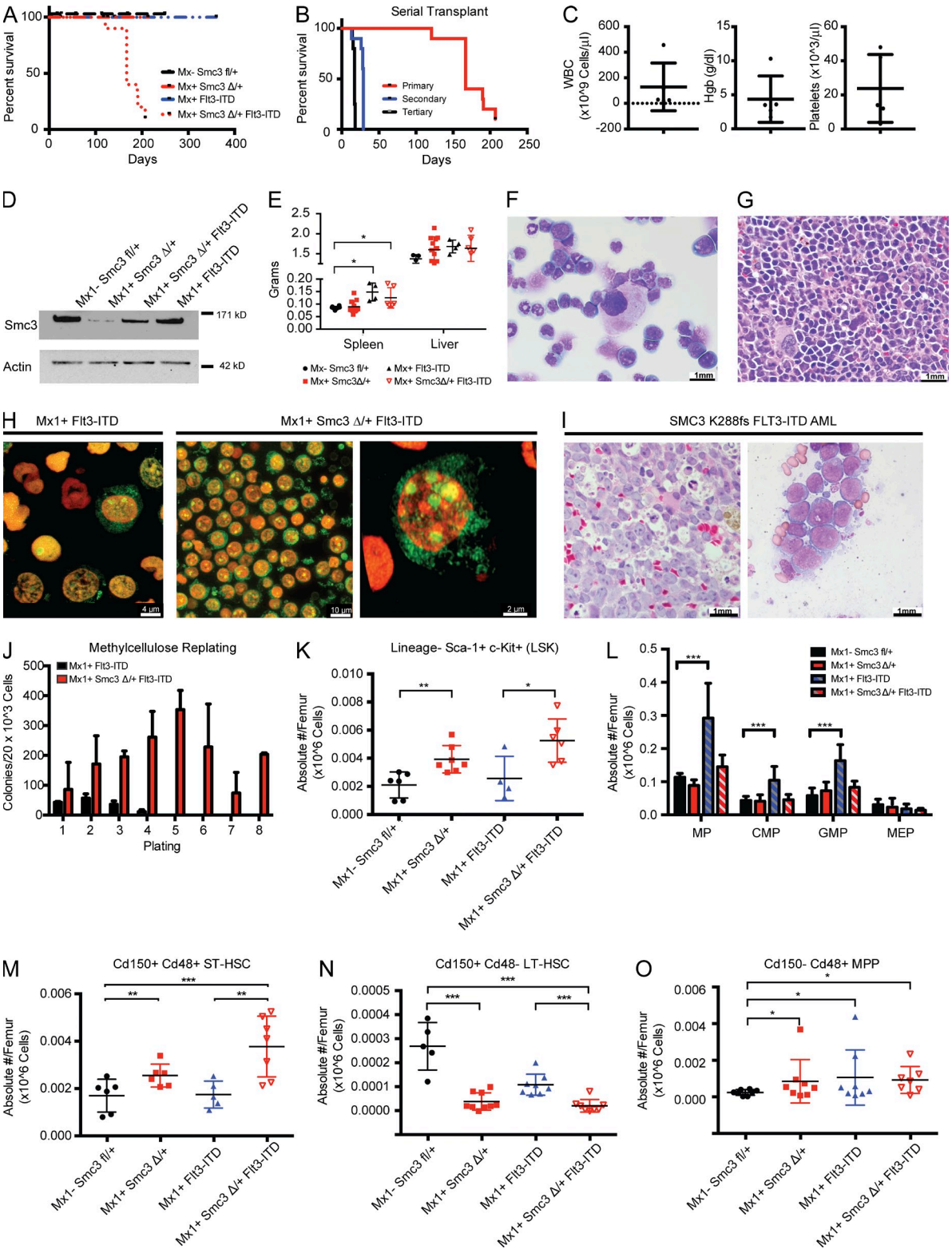

Figure 3. ***Smc3*** **haploinsufficiency cooperated with** ***Flt3*****-ITD to induce AML.** (A) Kaplan-Meier survival curve of primary transplant recipients of 10^6 total BM cells from $Smc3^{fl/+}$ ($n = 6$), $Smc3^{\Delta/+}$ ($n = 5$), $Flt3^{ITD}$ ($n = 5$), and $Smc3^{\Delta/+}$ $Flt3^{ITD}$ mice ($n = 5$). (B) Kaplan-Meier survival curve of secondary and tertiary transplantation of BM from $Smc3^{\Delta/+}$ $Flt3^{ITD}$ mice ($n = 5$ each). (C) Peripheral blood counts of secondary transplanted mice with BM from $Smc3^{fl/+}$ *Flt3*-ITD primary mice at the time of death ($n = 5$). (D) Mx1-cre–mediated deletion of one Smc3 allele reduces Smc3 expression in $Smc3^{\Delta/+}$ and $Smc3^{\Delta/+}$ $Flt3^{ITD}$ mice compared with age-matched controls ($Smc3^{fl/+}$ and $Flt3^{ITD}$). (E) Liver and spleen weights for primary mice ($n = 4$–8

These data suggest that concurrent *Flt3*-ITD mutation and *Smc3* heterozygosity alter the stem/progenitor milieu.

Smc3 haploinsufficiency results in a distinct reduction of mRNA transcriptional output

We performed RNA sequencing of poly-A selected transcripts (mRNA-seq) to measure global gene expression of c-Kit$^+$ hematopoietic progenitors 4 wk after conditional deletion of a single *Smc3* allele. Samples were harvested from individual mice, with a high correlation between samples of the same genotype. We hypothesized that *Smc3* haploinsufficiency would result in global and locus-specific effects on cis-regulatory elements influencing coordinated gene expression programs. We used standardized spiked-in synthetic RNAs to normalize RNA expression to the input cell number to allow us to discern the impact of *Smc3* haploinsufficiency on global patterns of gene expression (Lovén et al., 2013). When RNA expression changes were measured without input cell number normalization, modest effects on gene expression were observed with only a small proportion of genes significantly up- or down-regulated (Fig. 4 A). However, when the data were normalized to input cell number, we observed a significant decrease of a large subset of transcripts in *Smc3*$^{\Delta/+}$ hematopoietic cells (Fig. 4, B and C), consistent with a global reduction in transcription. Whereas the magnitude of global transcriptional dampening observed with *Smc3* haploinsufficiency was modest throughout the transcriptome (Fig. 4 C), we identified a subset of genes with disproportionate dysregulation of gene expression. We found a subset of genes to be significantly down-regulated (n = 644), whereas another subset of genes were relatively unchanged between genotypes (n = 364; Fig. 4 D and Table S1). We found that among the unchanged gene set were known regulators of stem cell maintenance, including *Hif1a* and *Tet2* (Ko et al., 2011; Kim et al., 2014). In contrast, we observed a marked decrease in the expression of genes indicative of lineage-committed cells, including the lymphoid-specific transcription factors *Pou2af1* and *Bcl3* and the myeloerythroid transcription factor *Gfi1b*. These data suggest that cohesin haploinsufficiency alters the transcriptional balance between stem cell self-renewal and lineage commitment.

To comprehensively explore transcriptional programs influenced by *Smc3* loss in an unbiased manner, we performed gene set enrichment analysis (GSEA) on the *Smc3*$^{fl/+}$ and *Smc3*$^{\Delta/+}$ RNA sequencing data (Subramanian et al., 2005). *Smc3* haploinsufficiency enriched for genes that are differentially expressed in human cord blood stem/progenitor cells (Fig. 4 E; Jaatinen et al., 2006). To further investigate the nature of the down-regulated gene set, we performed GSEA using this gene set searching for enrichment in a pairwise fashion with gene expression datasets from a compendium of mouse and human hematopoietic progenitor and lineage cells (Novershtern et al., 2011; Lara-Astiaso et al., 2014). We found that the down-regulated gene set was enriched not only in HSCs, but also in lineage-committed progenitor cells and differentiated hematopoietic cells (Fig. 4, F and G). Enrichment was especially apparent in megakaryocyte-erythrocyte progenitors (MEPs) and differentiated mouse erythrocytes (Ery) and also in the common lymphoid progenitor (CLP) population. However, these genes are specifically not enriched in myeloid cell types (granulocytes, monocytes, and macrophages). These data reveal that many of the genes most disrupted by cohesin haploinsufficiency are regulatory factors required for lineage commitment, mechanistically corroborating the increase in self-renewal and impaired differentiation with cohesin haploinsufficiency

Cohesin haploinsufficiency disrupts expression of genes with distinct chromatin organization

We next performed assays of transposase-accessible chromatin sequencing (ATAC-seq) on *Smc3*$^{fl/+}$ and *Smc3*$^{\Delta/+}$ cells. This allowed us to assess chromatin accessibility at transposase hypersensitive sites (THSs) across the *Smc3*$^{\Delta/+}$ genome compared with WT cells (Fig. 5 A). When THSs were analyzed based on specific genomic features (promoters and enhancers), we only observed a modest decrease in chromatin accessibility at enhancer regions. We then compared the local chromatin structure of down-regulated genes compared with unchanged genes. Surprisingly, chromatin structure at these genes remained largely unchanged, revealing that reduced *Smc3* levels did not dramatically change chromatin accessibility, even at gene loci that displayed significant decreases in mRNA levels. We observed at THSs outside of promoter regions, indicative of transcription factor–bound enhancer regulatory elements, that overall chromatin accessibility was lower at down-regulated gene loci compared with unchanged genes. To further explore chromatin characteristics that may indicate an increased susceptibility to reduced *Smc3* levels, we analyzed the density of chromatin accessibility immediately surrounding transcriptional start sites (TSSs) at the unchanged and down-regulated gene loci. We

for each genotype). (F and G) H&E stain of BM cytospin (F) and spleen (G). (H) Nucleolar stain of *Flt3*^{ITD} and *Smc3*$^{\Delta/+}$ *Flt3*^{ITD} BM. ACK-lysed BM was stained with TOTAL-NUCLEAR-ID fluorescent reagents, allowing simultaneous staining of both the nucleoli (green) and total nucleus (red). (I) H&E stain of MDS patient with refractory anemia with excess blasts-1 (RAEB-1) with molecular genetics identifying SMC3 K288fs and FLT3-ITD. Further experiments also identified IDH2 R140Q. Light microscopy at 100 magnification reveals multiple nucleoli in the blast population. (J) Serial plating and colony counts in methylcellulose for *Smc3*$^{\Delta/+}$ *Flt3*^{ITD} and *Flt3*^{ITD} BM. Whole BM was plated in triplicate at 20K cells/well. (K) Flow cytometric enumeration of BM LSK (Lin$^-$ Sca1$^+$ c-Kit$^+$). (L–O) enumeration of MPs (Lin$^-$ Sca1$^-$ c-Kit$^+$), CMPs (lineage$^-$ c-Kit$^+$ Sca-1$^-$ FcγR$^-$ CD34$^+$), GMPs (lineage$^-$ c-Kit$^+$ Sca-1$^-$ FcγR$^+$ CD34$^+$), and MEPs (lineage$^-$ c-Kit$^+$ Sca-1$^-$ FcγR$^-$ CD34$^-$; L) and flow cytometric enumeration of ST-HSCs (LSK Cd150$^+$ Cd48$^+$; M), LT-HSCs (LSK CD150$^+$ CD48$^-$; N), and MPP cells (LSK CD150$^-$ CD48$^+$; O; n = 5–8 mice per genotype). Data are expressed as frequency of live cells per femur. Error bars represent ± SD (C, E, and J–O); *, P < 0.05; **, P < 0.01; ***, P < 0.001 (Mann–Whitney U test).

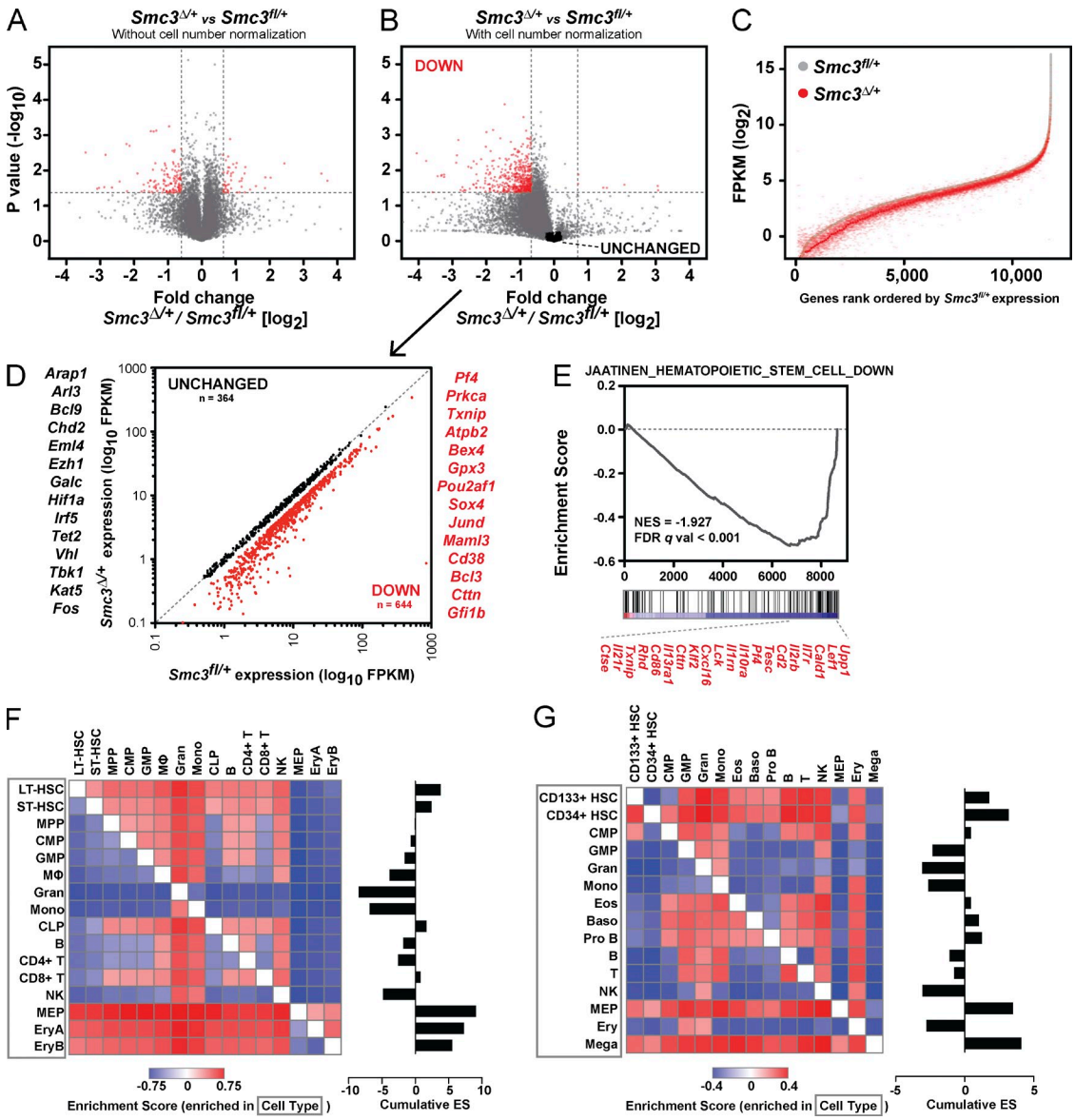

Figure 4. ***Smc3*** **haploinsufficiency perturbs mRNA transcriptional output.** RNA-seq using synthetic RNA spike-in controls reveals RNA transcript levels are globally decreased in $Smc3^{\Delta/+}$ c-Kit$^+$ cells when compared with $Smc3^{fl/+}$ WT. (A and B) The widespread decrease in overall mRNA levels is obscured when spike-in control reads are not used (A) but apparent with cell number normalization (B); fold change values represent the mean of duplicate samples. (C) These effects are apparent across gene expression levels; gray line represents gene expression of $Smc3^{fl/+}$ cells rank ordered by expression level; red dotted line represents LOESS curve through $Smc3^{\Delta/+}$ matched values. (D) Scatterplot of genes identified as unchanged and down-regulated with *Smc3* haploinsufficiency with exemplary genes in each group shown. Gene lists generated as defined in Materials and methods; full gene lists annotated in Table S1. (E) GSEA using a human hematopoietic progenitor gene set, with several enriched down-regulated genes highlighted. (F and G) Pairwise GSEA of mouse (F) and human (G) hematopoietic cells using the down-regulated gene set. Cumulative enrichment scores represent the sum of enrichment scores for each cell type when compared across all other cell types.

observed significantly less THS density surrounding TSSs of down-regulated genes when compared with unchanged genes (Fig. 5 B, left). This difference in ATAC-seq signal is observable within ∼30 kb in the 5′ direction and ∼10 kb in the 3′ direction of the TSS. This size domain generally corresponds to the size of typical local chromatin looping interactions that facilitate transcription factor–mediated transactivation, as observed by high-throughput chromatin conformation capture experiments in a variety of cell types (Jin et al., 2013). These data establish a model whereby promoters that are associated with fewer local cis-regulatory elements regulate genes most affected by cohesin complex depletion.

We next analyzed THS density of either enhancer- or promoter-specific sites. We did not observe significant THS density of other local promoter sites at either unchanged or down-regulated genes, indicating that the THS

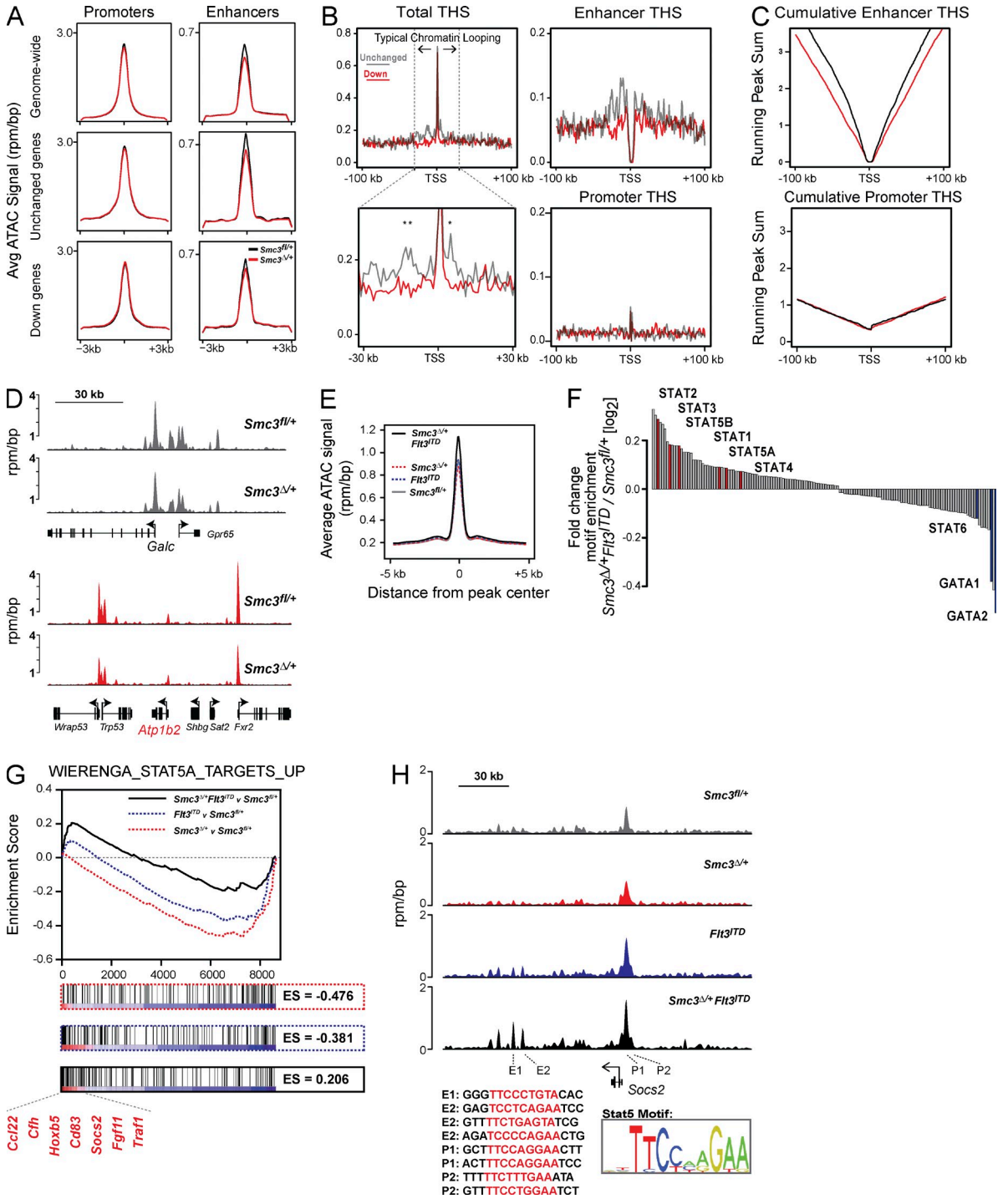

Figure 5. Chromatin accessibility profiles of *Smc3* haploinsufficiency. (A) Global chromatin accessibility assessed by ATAC-seq (top row). Overall THS density was analyzed genome wide and found in promoter regions (±1 kb of annotated RefSeq TSS) and enhancer sites (>1 kb from annotated TSS). All plots were generated using a LOESS curve through the mean of duplicate ATAC-seq measurements. Analysis was also performed on THSs of unchanged and down-regulated genes (middle and bottom rows). THSs included in analysis were within 30 kb of annotated TSSs of either unchanged or down-regulated genes. (B) ATAC-seq peak density was quantified within a 200-bp window of gene TSSs in 1-kb bins (top left). A highlighted 60-kb region immediately surrounding the TSSs is shown in the bottom left panel (* represents individual bins with $P < 0.005$, Student's *t* test). The value for each bin is the mean of replicate samples with a fitted LOESS curve. Enhancer-only THS density is shown in the top right panel, whereas promoter-only peaks are shown in the bottom right panel. (C) Cumulative THS enhancer and promoter peaks counting outwards from TSSs. (D) Chromatin accessibility of the unchanged gene locus *Galc* and the down-regulated gene locus *Atp1b2*. (E) Genome-wide chromatin accessibility at THSs as measured by ATAC-seq in each genotype. Plotted is the mean ATAC-seq signal at all THSs genome wide. (F) Transcription factor motif site enrichment

density differences we observe are not a result of a high density of active genes (Fig. 5 B, bottom right). In contrast, we found that THS density was specifically depleted at enhancer sites predominantly immediately upstream of the down-regulated gene set (Fig. 5 B, top right). In addition to decreased local THS enhancer density at down-regulated genes, we observed lower absolute numbers of enhancer, but not promoter, THSs within at 200-kb window of TSSs (Fig. 5 C). These analyses show that a particular subset of lineage commitment genes in HSCs are particularly reliant on normal expression levels of cohesin subunits and that their chromatin structure locally around the TSS has fewer enhancer elements. In contrast, genes with stable expression in the setting of *Smc3* attenuation have a greater THS density surrounding their promoter regions, suggesting *Smc3* haploinsufficiency does not disrupt the more complex promoter/enhancer interactions in these transcriptional complexes. For example, the *Galc* locus remains stable with *Smc3* haploinsufficiency and contains a large region of chromatin accessibility immediately upstream of its active promoter. In contrast, down-regulated genes such as *Atp1b2* have lower levels of chromatin accessibility at their locus, with fewer local enhancer THS sites (Fig. 5 D).

Combined *Smc3* haploinsufficiency and *Flt3*-ITD results in potentiation of Stat5-driven transcription

To investigate how *Smc3* haploinsufficiency may cooperate with the known myeloid leukemia oncogene *Flt3*-ITD to promote leukemia in mice, we analyzed the gene expression and chromatin accessibility profiles of c-Kit$^+$ hematopoietic cells from mice harboring $Flt3^{ITD}$ alone and in combination with *Smc3* monoallelic deletion. We found that THSs in $Smc3^{\Delta/+}$ $Flt3^{ITD}$ cells generally were more accessible than in cells of the other genotypes (Fig. 5 E). This suggests that the combination of $Smc3^{\Delta/+}$ and $Flt3^{ITD}$ in hematopoietic cells potentiates alterations in chromatin factor association through either gain or loss of functional cis-regulatory elements. To understand which TFs may be driving the observed increase in genome-wide chromatin accessibility, we analyzed 146 transcription factor recognition motifs within the THSs differentially observed in $Smc3^{\Delta/+}$ $Flt3^{ITD}$ and WT cells (Fig. 5 F). Notably, the THSs that are lost in the $Smc3^{\Delta/+}$ $Flt3^{ITD}$ cells are enriched in both Gata1- and Gata2-binding sites, whereas THSs that are gained in $Smc3^{\Delta/+}$ $Flt3^{ITD}$ cells are enriched in Stat family transcription factor–binding sites, including Stat5. As Flt3-ITD alters gene expression through the STAT transcription factors, we reason that increased accessibility at THS cis-regulatory elements and the alterations in gene expression seen in cells with combined *Smc3* haploinsufficiency and $Flt3^{ITD}$ may be in a large part driven by potentiated Stat signaling at chromatin. We next investigated the impact of combined *Smc3* haploinsufficiency and $Flt3^{ITD}$ on a STAT5 target gene expression signature derived from expression of activated STAT5A in human CD34$^+$ HSCs/progenitors (Wierenga et al., 2008). We observed enrichment of the STAT5A signature in the $Smc3^{\Delta/+}$ $Flt3^{ITD}$ cells compared with $Smc3^{\Delta/+}$, $Flt3^{ITD}$, and WT cells, suggesting the divergent mutations cooperate to potentiate oncogenic Stat5 signaling in HSCs (Fig. 5 G). Among the Stat5 target genes most differentially activated in our dataset is *Socs2*, a suppressor of cytokine signaling found to be up-regulated in AML patients, a known target gene of the STAT5 transcription factor, and a marker of poor prognosis (Laszlo et al., 2014). We observed increased chromatin accessibility at enhancer THSs at the *Socs2* locus in both $Flt3^{ITD}$ mutant hematopoietic cells and, at a greater magnitude, in $Smc3^{\Delta/+}$ $Flt3^{ITD}$ cells (Fig. 5 H). These data suggest that the lower *Smc3* level in these cells potentiates Stat5 chromatin association at the locus, perhaps by establishing a more permissive chromatin architecture, thus increasing accessibility for Stat5 binding. Using the TCGA dataset for de novo AML (Cancer Genome Atlas Research Network, 2013), we assessed gene expression changes in non-APL cohesin mutant AML compared with FLT3-ITD, cohesin WT AML patients. Similar to our mouse results, cohesin mutant AML had increased *SOCS2* expression (Log2 fold change 2.2, false discovery rate $< 3.64 \times 10^{-6}$).

Gene discovery studies have identified somatic, loss of function mutations in most major subunits of the cohesin complex, including *STAG2*, *SMC1A*, *SMC3*, and *RAD21*, in patients with myeloid malignancies such as MDS and AML (Jan et al., 2012; Welch et al., 2012; Cancer Genome Atlas Research Network, 2013; Kon et al., 2013; Thol et al., 2014; Thota et al., 2014). These mutations are almost always monoallelic and mutually exclusive, suggesting that proper cohesin function in HSCs requires a specific dosage, which is altered in myeloid transformation. Here we demonstrate a dose-dependent requirement for *Smc3* in hematopoiesis and in stem cell function. Whereas biallelic loss of *Smc3* abrogates HSC function, heterozygous loss of *Smc3* increases HSC function and alters the balance toward self-renewal at the expense of lineage commitment. These data underscore the critical role for cohesin in regulating cell specification during pivotal developmental transitions in hematopoietic cells. In addition, our data are consistent with the clinical observation that cohesin mutations are not associated with chromosomal instability, but rather alter the chromatin state and transcriptional output of hematopoietic cells.

Smc3 haploinsufficiency results in an expansion of stem/progenitor cells in the BM coupled with dysmegakaryopoiesis, which are seen in chronic myeloid malignancies such as

in ATAC-seq peaks gained and lost in $Smc3^{\Delta/+}$ *Flt3*-ITD cells compared with $Smc3^{fl/+}$. (G) GSEA using RNA-seq data from each genotype compared with $Smc3^{fl/+}$ controls and a human HSC STAT5 target gene set. (H) Chromatin accessibility of the Stat5 target gene *Socs2* showing potentiation of Stat5 signaling at specific regulatory elements. Shown are ATAC-seq profiles of the entire locus for each genotype. Stat5 motifs are found within each labeled regulatory element (sequence highlighted in red).

MDS and in preleukemic clonal hematopoiesis (Welch et al., 2012; Jaiswal et al., 2014). Moreover, *Smc3* haploinsufficient cells showed a capacity for serial replating and competitive advantage in BM transplant assays, consistent with an increase in self-renewal. Consistent with these data, we observed marked alterations in the transcriptome of *Smc3* haploinsufficient stem/progenitor cells. The majority of differentially expressed genes were down-regulated, including marked reduction in the expression of genes involved in lineage priming such as *Pou2af1* and *Gfi1b*. The specific loss of lineage factors, normally expressed at constitutive levels in early stem/progenitor cells, likely constrains the capability of these cells to commit to downstream lineages.

The majority of genes that showed altered expression in *Smc3* haploinsufficient cells show decreased RNA expression, in concordance with the notion that the cohesin complex plays an important role in maintaining active transcription complexes. Importantly, the genes that were not altered with cohesin attenuation shared chromatin characteristics that suggest locally complex transcriptional regulatory domains are relatively resistant to reduced *Smc3* expression. This is in contrast to other recent studies where near-complete disruption of cohesin subunit expression more symmetrically alters gene expression, including increased expression of many target genes (Ing-Simmons et al., 2015). Our data suggest that this level of *Smc3* expression is sufficient to maintain most transcription regulatory elements to a degree required for HSC proliferation and self-renewal, while reducing the expression of genes required for lineage determination and differentiation. The genes that maintain stem cell identity are often characterized by highly complex regulatory elements with several promoter–enhancer and enhancer–enhancer contacts in the form of so-called "super-enhancers" (Whyte et al., 2013). Although these complex regulatory elements may be sensitive to disruption of cohesin complexes, in normal hematopoiesis cohesin may be titrated at a higher efficiency to these elements by DNA-binding transcription factors like CTCF than more "typical" enhancers at less complexly regulated loci. In contrast, the factors that govern lineage determination may have less complex transcriptional regulation in the stem cell state, which is lost with reduced cohesin expression.

The observation that cohesin mutations can co-occur with tyrosine kinase mutations in AML led us to perform experiments that showed that *Smc3* monoallelic deletion cooperates with *Flt3*-ITD to induce AML in vivo. We have recently shown cooperativity between a chromatin-associated mutant allele (*Tet2*) and $Flt3^{ITD}$ in inducing AML in a mouse model (Shih et al., 2015). Notably, similar effects on gene expression were observed in our current, cohesin mutant AML model, including loss of *Gata1* and *Gata2* regulation and up-regulation of *Socs2*. These data suggest cohesin mutations can confer a chromatin structure permissive to oncogenic signaling from growth factor–independent and somatically altered oncogenes. Mechanistically, combined *Smc3* and *Flt3* mutations resulted in potentiation of Stat5-mediated transcriptional output. Although *Flt3*-ITD has been shown to activate Stat5 nuclear localization and transactivation activity (Hayakawa et al., 2000; Mizuki et al., 2000; Zhang et al., 2000), the combination with *Smc3* haploinsufficiency increased the expression of Stat5 targets by altering chromatin structures at Stat5-binding motifs. This potentiation may be a result of relaxed chromatin architecture, which allows for increased Stat5 chromatin association in the setting of mutant-driven kinase activation.

Interestingly, we observed a preponderance of disrupted multifocal nucleoli present in $Smc3^{\Delta/+}$ and, to a greater extent, in $Smc3^{\Delta/+}$ $Flt3^{ITD}$ hematopoietic progenitors. This phenotype resembles the nucleolar alterations seen in Roberts syndrome, a known cohesinopathy. There, mutation in the human *ESCO2* gene inactivates the SMC3 acetyltransferase required to induce cohesiveness of the cohesin ring complex (Harris et al., 2014). Roberts syndrome nuclei display strikingly similar gross nucleolar architecture, with disrupted ribosomal RNA expression and ribosome biogenesis. Thus, we speculate that leukemogenesis facilitated by reduction in functional cohesin complexes may also arise as a result of disrupted protein synthesis pathways in addition to perturbed gene expression. Most provocatively, our data showing that complete loss of cohesin complex abrogates hematopoiesis suggest a potential therapeutic opportunity in disrupting cohesin function in *Smc3* haploinsufficient malignancies. Subsequent studies are required to delineate whether malignancies that feature cohesin haploinsufficiency as a mechanism of transformation are sensitive to further attenuation of cohesin function and whether this can be leveraged to therapeutic benefit.

MATERIALS AND METHODS

Animals. All animals were housed at Memorial Sloan Kettering Cancer Center. All animal procedures were conducted in accordance with the Guidelines for the Care and Use of Laboratory Animals and were approved by the Institutional Animal Care and Use Committees at Memorial Sloan Kettering Cancer Center.

Generation of Smc3-deficient mice. The *Smc3* allele was deleted by targeting exon 4 in a construct obtained from the EUCOMM consortium (*Smc3*$^{tm1a(EUCOMM)Wtsi}$). Two *LoxP* sites flanking exon 4 and an *Frt*-flanked neomycin selection cassette were inserted in the upstream intron (Fig. 1 A). Positive embryonic stem clones were expanded and injected into blastocysts. The generated mice ($Smc3^{fl/fl}$) were initially crossed to a germline *Flp*-deleter (The Jackson Laboratory), to eliminate the neomycin cassette, and subsequently to the IFN-α–inducible *Mx1-cre* (The Jackson Laboratory; Kühn et al., 1995; Lakso et al., 1996). Mice were backcrossed for six generations to C57BL/6 mice. $Smc3^{fl/fl}$, $Smc3^{fl/+}$, and $Smc3^{+/+}$ littermate mice were genotyped by PCR with primers Smc3-FloxF (5′-TGTTGCCTCCCTGTGTTCTCAGGC-3′), Smc3-CommonF (5′-TCTTCGTCCAGAGCAGCGATTGGC-3′), and Smc3-CommonR (5′-TGAGCCATCATGTGGATGCT-3′) using the following parameters: 95°C for 4 min, followed by 35 cycles of 95°C for 45 s, 56°C for 45 s, and 72°C for 1 min, and then 72°C for 5 min. The WT allele was detected as a band at 287 bp, whereas the floxed allele was detected as a band of 313 bp. Excision after Cre recombination was confirmed by PCR with primers to detect a band at 349 bp.

In vivo experiments. *Mx1-cre* $Smc3^{fl/fl}$ conditional and Cre^{-} $Smc3^{fl/fl}$ control mice received four intraperitoneal injections of PIpC every other day at a dose of 20 mg/kg of body weight starting at 2 wk after birth. Mice were analyzed between 1 and 60 wk of age. BM, spleen, and peripheral blood

were analyzed by flow cytometry. Formalin-fixed paraffin-embedded tissue sections were stained with hematoxylin and eosin (H&E). Peripheral blood was smeared on a slide and stained using the Wright-Giemsa staining method. Tissue sections and blood smears were evaluated by a hematopathologist (A. Chiu). Deletion of the *Smc3* allele and transcript was measured by genomic PCR and Western blot analysis.

BM transplantation. Freshly dissected femurs and tibias were isolated from *Smc3*$^{fl/fl}$ CD45.2$^+$ or *Mx1-cre*$^+$ *Smc3*$^{fl/fl}$ CD45.2$^+$ mice. BM was flushed with a 3-cc insulin syringe into PBS supplemented with 3% FBS. The BM was spun at 0.5 *g* by centrifugation at 4°C, and RBCs were lysed in ACK bicarbonate lysis buffer for 5 min. After centrifugation, cells were resuspended in PBS plus 3% FBS, passed through a cell strainer, and counted. Finally, 0.5 × 10^6 total BM cells from *Smc3*$^{fl/fl}$ CD45.2$^+$ or *Mx1-cre*$^+$ *Smc3*$^{fl/fl}$ CD45.2$^+$ mice were mixed with 0.5 × 10^6 WT CD45.1$^+$ support BM and transplanted via tail vein injection into lethally irradiated (two times 450 cGy) CD45.1$^+$ host mice. Chimerism was measured by FACS in peripheral blood at 2 wk after transplant (week 0, pre-PIpC). Chimerism was followed via FACS in the peripheral blood every 4 wk (week 0, 4, 6, 8, 12, 16, and 20 after PIpC injection). Additionally, for each bleeding, whole blood cell counts were measured on a blood analyzer, and peripheral blood smears were scored. Chimerism in the BM, spleen, and thymus was evaluated at 20 wk via animal sacrifice and subsequent FACS analysis. The above procedure was also repeated with *Smc3*$^{fl/+}$ CD45.2$^+$, *Mx1-cre*$^+$ *Smc3*$^{fl/+}$ CD45.2$^+$ mice for competitive transplantation of mice with monoallelic loss of *Smc3*. For noncompetitive serial transplantation experiments, 10^6 total BM cells of *Smc3*$^{fl/+}$ *Flt3*^{ITD} CD45.2$^+$ mice were injected into lethally irradiated (two times 450 cGy) CD45.1$^+$ host mice. Recipient mice were then followed until moribund.

In vitro colony-forming assays. BM of *Smc3*$^{fl/+}$ and littermate *Mx1-cre* *Smc3*$^{\Delta/+}$ mice was seeded at a density of 20,000 cells/replicate into cytokine-supplemented methylcellulose medium (MethoCult M3434; STEMCELL Technologies). Colonies propagated in culture were scored at day 7. Representative colonies were isolated from the plate for cytospins and flow cytometry. Remaining cells were resuspended and counted, and a portion was taken for replating (20,000 cells/replicate) for a total of seven platings. Cytospins were performed by resuspending in warm PBS and spinning onto the slides at 350 *g* for 5 min. Slides were air-dried and stained using the Giemsa-Wright method.

Antibodies, FACS, and Western blot analysis. Antibody staining and FACS analysis were performed as previously described (Abdel-Wahab et al., 2013). BM or spleen mononuclear cells were stained with a lineage cocktail comprised of antibodies targeting CD4, CD8, B220, NK1.1, Gr-1, CD11b, Ter119, and IL-7Rα. Cells were also stained with antibodies against c-Kit, Sca-1, FcγRII/III, and CD34. Cell populations were analyzed using a FACS-LSRII (BD) and sorted with a FACSAria instrument (BD). All antibodies were purchased from BD or eBioscience. We used the following antibodies: c-Kit (2B8), Sca-1 (D7), Mac-1/CD11b (M1/70), Gr-1 (RB6-8C5), NK1.1 (PK136), Ter-119, IL7-Rα (A7R34), CD34 (RAM34), FcγRII/III (2.4G2), CD4 (RM4-5), CD4 (H129.19), CD8 (53-6.7), CD45.1 (A20), CD45.2 (104), CD150 (9D1), and CD48 (HM48-1). The following antibodies were used for Western blot analysis: Smc3 (Bethyl Laboratories, Inc.) and Actin (EMD Millipore).

Nucleolar detection analyses. Mouse BM was washed with PBS, and 1.5 × 10^6 cells were centrifuged at 400 *g* for 5 min and then stained with 50 µl of dual detection reagent TOTAL-NUCLEAR-ID (Enzo Life Sciences). Cells were incubated for 30 min at 37°C and then washed with 200 µl of 1× buffer solution. Cells were centrifuged at 400 *g* for 5 min and resuspended in 200 µl of 1× buffer solution and seeded into an 8-well chamber slide (Lab-Tek). Z-stack images were taken using a TCS SP8 confocal laser-scanning microscope (Leica) equipped with a 63× objective. Images were deconvolved and processed using Imaris 3D software (Bitplane AG).

Histological analyses. Mice were sacrificed and autopsied, and then dissected tissue samples were fixed for 24 h in 4% paraformaldehyde, dehydrated, and embedded in paraffin. Paraffin blocks were sectioned at 4 µm and stained with H&E. Images were acquired using an Axio Observer A1 microscope (Carl Zeiss).

Peripheral blood analysis. Blood was collected by retroorbital bleeding using heparinized microhematocrit capillary tubes (Thermo Fisher Scientific). Automated peripheral blood counts were obtained using a ProCyte Dx (IDEXX Laboratories) according to standard manufacturer's instruction. Differential blood counts were realized on blood smears stained using Wright-Giemsa staining and visualized using an Axio Observer A1 microscope.

Cytogenetic analysis and metaphase karyotyping. BM aspirates after documented excision or day 5 after PIpC (for *Smc3*$^{\Delta/\Delta}$) were injected into T25 flasks containing 5 ml RPMI 10% FCS supplemented with 2 mM L-glutamine. Harvested cells were cultured with 25 µl colcemid (10 mg/ml; Gibco) for 45 min and 4 h, respectively, resuspended in 0.075 mol/l KCl for 10 min at 37°C, and fixed in methanol/acetic acid (3:1). Metaphases were scored and counted. Chromosome analysis was performed on a minimum of 20 DAPI-banded metaphases, and all metaphases were fully karyotyped.

RNA-seq and quantitative real-time PCR (qRT-PCR) analysis. For qRT-PCR experiments, all samples were prepared in biological triplicate. Whole BM was positively selected for Cd117 (c-Kit) using antibodies conjugated to magnetic beads and separated over a column (Cd117 microbeads; Miltenyi Biotec). Total RNA was isolated using TRIzol (Invitrogen), and cDNA was synthesized using the SuperScript First-Strand kit (Invitrogen). Quantitative PCR was performed using SYBR green iMaster and a LightCycler 480 (Roche). For mRNA-seq analysis, samples were prepared and analyzed in biological duplicate (r^2 = 0.9724, *Smc3*$^{fl/+}$ sample 1 vs. 2; 0.9809, *Smc3*$^{\Delta/+}$ sample 1 vs. 2; 0.9760, *Flt3*^{ITD} sample 1 vs. 2; 0.9401, *Smc3*$^{\Delta/+}$ *Flt3*^{ITD} sample 1 vs. 2). We used ERCC RNA Spike-In Mix (Life Technologies) for cell number normalization. Fastq files were aligned to mm9 using HiStat with default parameters. Transcript abundances were calculated using the cuffquant module of Cufflinks. FPKM values were calculated and normalized using Cuffnorm. We considered genes that had a $P < 0.05$ and $\log_2$ fold change value ≤0.58 to be significantly down-regulated between genotypes. To determine "unchanged" genes between genotypes, we considered genes with <25% variance between replicates and $\log_2$ fold changes <0.2. GSEA was performed using default parameters with the following exceptions: -nperm 1000, -rnd_seed 149, -set_max 1500, -norm meandiv. RNA-seq data are deposited in NCBI's GEO database, accessible through accession no. GSE73218.

ATAC-seq. Chromatin accessibility assays using the bacterial Tn5 transposase were performed as described previously (Buenrostro et al., 2013) with minor modifications. For ATAC-seq analysis, samples were prepared and analyzed in biological duplicate. 50 × 10^3 cells were lysed and incubated with transposition reaction mix for 60 min at 37°C. Samples were PCR amplified and sequenced on a NextSeq 500 (Ilumina). Fastq files were aligned to mm9 with Bowtie, and peaks were called using Zinba. ATAC peak density near unchanged versus down-regulated gene TSSs was determined by extending the TSS region by 100 kb in the 5′ and 3′ direction. The 200-kb window was binned into 1-kb regions, and overlapping ATAC peaks in each window were counted. Regions were further subdivided into regions overlapping enhancers or promoters. The mean ATAC peak density in each window across each gene set was plotted as a function of distance from the TSS. A LOESS fit line was added to capture overall trends. Density plots were determined by binning 3- or 5-kb windows centered at ATAC peaks into 200 50-bp bins. Signal density at each region was calculated, and the mean density in that region was plotted in units of reads per million per base pair (rpm/bp). Transcription factor motif analysis was performed using the FIMO database of the MEME suite. Transcription factor motif densities were calculated for pairwise comparisons of unique ATAC peaks for motifs with annotated position

weight matrices (PWMs; Matys et al., 2006). To generate expected motif background frequencies, ATAC-enriched regions were, respectively, scrambled to maintain dinucleotide frequencies akin to the actual genomic sequences. Motifs were considered present in these regions if they had >1.5-fold change between observed frequency ratios in unique ATAC-enriched regions and a p-value <0.05 for each pairwise comparison. The statistical significance of differences of motif occurrences between genotypes was assessed using Fisher's exact test. ATAC-seq data are deposited in NCBI's GEO database, accessible through accession no. GSE73218.

Online supplemental material. Video 1 shows *Smc3*$^{fl/+}$ BM nucleolar 3D reconstruction. Video 2 shows *Smc3*$^{\Delta/+}$ *Flt3*-ITD BM nucleolar 3D reconstruction. Table S1, included as a separate Excel file, shows the *Smc3*$^{\Delta/+}$ stable and unstable gene list. Online supplemental material is available at http://www.jem.org/cgi/content/full/jem.20151317/DC1.

We would like to thank Dr. Katia Manova and the staff of the Molecular Cytology Core Facility for their assistance in imaging and processing of microscopy data and the Memorial Sloan Kettering Center Support Grant (P30 CA008748).

This work was supported by a grant from the Pershing Square Sohn Prize for Cancer Research (to R.L. Levine); a Damon Runyon Cancer Research Foundation Postdoctoral Fellowship Award, an American Society of Hematology Research Training Award for Fellows, an NCI Training Grant, Clinical Scholars Biomedical Research Training Program (T32 CA009512), and philanthropic support from the Dana Foundation and Lymphoma Foundation (to A.D. Viny); and a Research Fellow Award from the Leukemia and Lymphoma Society and an NCI Pathway to Independence Award (K99CA190861; to C.J. Ott).

The authors declare no competing financial interests.

Author contributions: Conceptualization, A.D. Viny, C.J. Ott, J.E. Bradner, and R.L. Levine. Methodology, A.D. Viny, C.J. Ott, B. Spitzer, M. Rivas, C. Meydan, J. Reyes, A. Chiu, Y. Romin, V. Boyko, A. Melnick, J.E. Bradner, and R.L. Levine. Investigation, A.D. Viny, C.J. Ott, E. Papalexi, D. Yelin, K. Shank, J.E. Bradner, and R.L. Levine. Writing the original draft, A.D. Viny and C.J. Ott. Writing: review, and editing, J.E. Bradner and R.L. Levine. Funding acquisition, J.E. Bradner and R.L. Levine. Resources, S. Thota, J.P. Maciejewski, A. Melnick, J.E. Bradner, and R.L. Levine. Supervision, J.E. Bradner and R.L. Levine.

Submitted: 16 August 2015
Accepted: 4 September 2015

REFERENCES

Abdel-Wahab, O., J. Gao, M. Adli, A. Dey, T. Trimarchi, Y.R. Chung, C. Kuscu, T. Hricik, D. Ndiaye-Lobry, L.M. Lafave, et al. 2013. Deletion of Asxl1 results in myelodysplasia and severe developmental defects in vivo. *J. Exp. Med.* 210:2641–2659. http://dx.doi.org/10.1084/jem.20131141

Balbás-Martínez, C., A. Sagrera, E. Carrillo-de-Santa-Pau, J. Earl, M. Márquez, M. Vazquez, E. Lapi, F. Castro-Giner, S. Beltran, M. Bayés, et al. 2013. Recurrent inactivation of STAG2 in bladder cancer is not associated with aneuploidy. *Nat. Genet.* 45:1464–1469. http://dx.doi.org/10.1038/ng.2799

Bell, A.C., A.G. West, and G. Felsenfeld. 1999. The protein CTCF is required for the enhancer blocking activity of vertebrate insulators. *Cell.* 98:387–396. http://dx.doi.org/10.1016/S0092-8674(00)81967-4

Buenrostro, J.D., P.G. Giresi, L.C. Zaba, H.Y. Chang, and W.J. Greenleaf. 2013. Transposition of native chromatin for fast and sensitive epigenomic profiling of open chromatin, DNA-binding proteins and nucleosome position. *Nat. Methods.* 10:1213–1218. http://dx.doi.org/10.1038/nmeth.2688

Cancer Genome Atlas Research Network. 2013. Genomic and epigenomic landscapes of adult de novo acute myeloid leukemia. *N. Engl. J. Med.* 368:2059–2074. http://dx.doi.org/10.1056/NEJMoa1301689

Dawson, M.A., T. Kouzarides, and B.J. Huntly. 2012. Targeting epigenetic readers in cancer. *N. Engl. J. Med.* 367:647–657. http://dx.doi.org/10.1056/NEJMra1112635

Dowen, J.M., Z.P. Fan, D. Hnisz, G. Ren, B.J. Abraham, L.N. Zhang, A.S. Weintraub, J. Schuijers, T.I. Lee, K. Zhao, and R.A. Young. 2014. Control of cell identity genes occurs in insulated neighborhoods in mammalian chromosomes. *Cell.* 159:374–387. http://dx.doi.org/10.1016/j.cell.2014.09.030

Harris, B., T. Bose, K.K. Lee, F. Wang, S. Lu, R.T. Ross, Y. Zhang, S.L. French, A.L. Beyer, B.D. Slaughter, et al. 2014. Cohesion promotes nucleolar structure and function. *Mol. Biol. Cell.* 25:337–346. http://dx.doi.org/10.1091/mbc.E13-07-0377

Hayakawa, F., M. Towatari, H. Kiyoi, M. Tanimoto, T. Kitamura, H. Saito, and T. Naoe. 2000. Tandem-duplicated Flt3 constitutively activates STAT5 and MAP kinase and introduces autonomous cell growth in IL-3-dependent cell lines. *Oncogene.* 19:624–631. http://dx.doi.org/10.1038/sj.onc.1203354

Ing-Simmons, E., V.C. Seitan, A.J. Faure, P. Flicek, T. Carroll, J. Dekker, A.G. Fisher, B. Lenhard, and M. Merkenschlager. 2015. Spatial enhancer clustering and regulation of enhancer-proximal genes by cohesin. *Genome Res.* 25:504–513. http://dx.doi.org/10.1101/gr.184986.114

Jaatinen, T., H. Hemmoranta, S. Hautaniemi, J. Niemi, D. Nicorici, J. Laine, O. Yli-Harja, and J. Partanen. 2006. Global gene expression profile of human cord blood–derived CD133$^+$ cells. *Stem Cells.* 24:631–641. http://dx.doi.org/10.1634/stemcells.2005-0185

Jaiswal, S., P. Fontanillas, J. Flannick, A. Manning, P.V. Grauman, B.G. Mar, R.C. Lindsley, C.H. Mermel, N. Burtt, A. Chavez, et al. 2014. Age-related clonal hematopoiesis associated with adverse outcomes. *N. Engl. J. Med.* 371:2488–2498. http://dx.doi.org/10.1056/NEJMoa1408617

Jan, M., T.M. Snyder, M.R. Corces-Zimmerman, P. Vyas, I.L. Weissman, S.R. Quake, and R. Majeti. 2012. Clonal evolution of preleukemic hematopoietic stem cells precedes human acute myeloid leukemia. *Sci. Transl. Med.* 4:149ra118. http://dx.doi.org/10.1126/scitranslmed.3004315

Jin, F., Y. Li, J.R. Dixon, S. Selvaraj, Z. Ye, A.Y. Lee, C.A. Yen, A.D. Schmitt, C.A. Espinoza, and B. Ren. 2013. A high-resolution map of the three-dimensional chromatin interactome in human cells. *Nature.* 503:290–294. http://dx.doi.org/10.1038/nature12644

Kagey, M.H., J.J. Newman, S. Bilodeau, Y. Zhan, D.A. Orlando, N.L. van Berkum, C.C. Ebmeier, J. Goossens, P.B. Rahl, S.S. Levine, et al. 2010. Mediator and cohesin connect gene expression and chromatin architecture. *Nature.* 467:430–435. http://dx.doi.org/10.1038/nature09380

Kim, W., K.D. Klarmann, and J.R. Keller. 2014. Gfi-1 regulates the erythroid transcription factor network through Id2 repression in murine hematopoietic progenitor cells. *Blood.* 124:1586–1596. http://dx.doi.org/10.1182/blood-2014-02-556522

Ko, M., H.S. Bandukwala, J. An, E.D. Lamperti, E.C. Thompson, R. Hastie, A. Tsangaratou, K. Rajewsky, S.B. Koralov, and A. Rao. 2011. Ten-Eleven-Translocation 2 (TET2) negatively regulates homeostasis and differentiation of hematopoietic stem cells in mice. *Proc. Natl. Acad. Sci. USA.* 108:14566–14571. http://dx.doi.org/10.1073/pnas.1112317108

Kon, A., L.Y. Shih, M. Minamino, M. Sanada, Y. Shiraishi, Y. Nagata, K. Yoshida, Y. Okuno, M. Bando, R. Nakato, et al. 2013. Recurrent mutations in multiple components of the cohesin complex in myeloid neoplasms. *Nat. Genet.* 45:1232–1237. http://dx.doi.org/10.1038/ng.2731

Kühn, R., F. Schwenk, M. Aguet, and K. Rajewsky. 1995. Inducible gene targeting in mice. *Science.* 269:1427–1429. http://dx.doi.org/10.1126/science.7660125

Lakso, M., J.G. Pichel, J.R. Gorman, B. Sauer, Y. Okamoto, E. Lee, F.W. Alt, and H. Westphal. 1996. Efficient in vivo manipulation of mouse genomic sequences at the zygote stage. *Proc. Natl. Acad. Sci. USA.* 93:5860–5865. http://dx.doi.org/10.1073/pnas.93.12.5860

Lara-Astiaso, D., A. Weiner, E. Lorenzo-Vivas, I. Zaretsky, D.A. Jaitin, E. David, H. Keren-Shaul, A. Mildner, D. Winter, S. Jung, et al. 2014. Chromatin state dynamics during blood formation. *Science.* 345:943–949. http://dx.doi.org/10.1126/science.1256271

Laszlo, G.S., R.E. Ries, C.J. Gudgeon, K.H. Harrington, T.A. Alonzo, R.B. Gerbing, S.C. Raimondi, B.A. Hirsch, A.S. Gamis, S. Meshinchi, and R.B. Walter. 2014. High expression of suppressor of cytokine signaling-2 predicts poor outcome in pediatric acute myeloid leukemia: a report from the Children's Oncology Group. *Leuk. Lymphoma.* 55:2817–2821. http://dx.doi.org/10.3109/10428194.2014.893305

Lee, B.H., Z. Tothova, R.L. Levine, K. Anderson, N. Buza-Vidas, D.E. Cullen, E.P. McDowell, J. Adelsperger, S. Fröhling, B.J. Huntly, et al. 2007. FLT3 mutations confer enhanced proliferation and survival

properties to multipotent progenitors in a murine model of chronic myelomonocytic leukemia. *Cancer Cell*. 12:367–380. http://dx.doi.org/10.1016/j.ccr.2007.08.031

Lovén, J., H.A. Hoke, C.Y. Lin, A. Lau, D.A. Orlando, C.R. Vakoc, J.E. Bradner, T.I. Lee, and R.A. Young. 2013. Selective inhibition of tumor oncogenes by disruption of super-enhancers. *Cell*. 153:320–334. http://dx.doi.org/10.1016/j.cell.2013.03.036

Matys, V., O.V. Kel-Margoulis, E. Fricke, I. Liebich, S. Land, A. Barre-Dirrie, I. Reuter, D. Chekmenev, M. Krull, K. Hornischer, et al. 2006. TRANSFAC and its module TRANSCompel: transcriptional gene regulation in eukaryotes. *Nucleic Acids Res.* 34:D108–D110. http://dx.doi.org/10.1093/nar/gkj143

Merkenschlager, M., and D.T. Odom. 2013. CTCF and cohesin: linking gene regulatory elements with their targets. *Cell*. 152:1285–1297. http://dx.doi.org/10.1016/j.cell.2013.02.029

Mizuki, M., R. Fenski, H. Halfter, I. Matsumura, R. Schmidt, C. Müller, W. Grüning, K. Kratz-Albers, S. Serve, C. Steur, et al. 2000. Flt3 mutations from patients with acute myeloid leukemia induce transformation of 32D cells mediated by the Ras and STAT5 pathways. *Blood*. 96:3907–3914.

Novershtern, N., A. Subramanian, L.N. Lawton, R.H. Mak, W.N. Haining, M.E. McConkey, N. Habib, N. Yosef, C.Y. Chang, T. Shay, et al. 2011. Densely interconnected transcriptional circuits control cell states in human hematopoiesis. *Cell*. 144:296–309. http://dx.doi.org/10.1016/j.cell.2011.01.004

Parelho, V., S. Hadjur, M. Spivakov, M. Leleu, S. Sauer, H.C. Gregson, A. Jarmuz, C. Canzonetta, Z. Webster, T. Nesterova, et al. 2008. Cohesins functionally associate with CTCF on mammalian chromosome arms. *Cell*. 132:422–433. http://dx.doi.org/10.1016/j.cell.2008.01.011

Rubio, E.D., D.J. Reiss, P.L. Welcsh, C.M. Disteche, G.N. Filippova, N.S. Baliga, R. Aebersold, J.A. Ranish, and A. Krumm. 2008. CTCF physically links cohesin to chromatin. *Proc. Natl. Acad. Sci. USA*. 105:8309–8314. http://dx.doi.org/10.1073/pnas.0801273105

Schaaf, C.A., H. Kwak, A. Koenig, Z. Misulovin, D.W. Gohara, A. Watson, Y. Zhou, J.T. Lis, and D. Dorsett. 2013. Genome-wide control of RNA polymerase II activity by cohesin. *PLoS Genet*. 9:e1003382. http://dx.doi.org/10.1371/journal.pgen.1003382

Shih, A.H., Y. Jiang, C. Meydan, K. Shank, S. Pandey, L. Barreyro, I. Antony-Debre, A. Viale, N. Socci, Y. Sun, et al. 2015. Mutational cooperativity linked to combinatorial epigenetic gain of function in acute myeloid leukemia. *Cancer Cell*. 27:502–515. http://dx.doi.org/10.1016/j.ccell.2015.03.009

Solomon, D.A., T. Kim, L.A. Diaz-Martinez, J. Fair, A.G. Elkahloun, B.T. Harris, J.A. Toretsky, S.A. Rosenberg, N. Shukla, M. Ladanyi, et al. 2011. Mutational inactivation of STAG2 causes aneuploidy in human cancer. *Science*. 333:1039–1043. http://dx.doi.org/10.1126/science.1203619

Stedman, W., H. Kang, S. Lin, J.L. Kissil, M.S. Bartolomei, and P.M. Lieberman. 2008. Cohesins localize with CTCF at the KSHV latency control region and at cellular c-myc and H19/Igf2 insulators. *EMBO J*. 27:654–666. http://dx.doi.org/10.1038/emboj.2008.1

Subramanian, A., P. Tamayo, V.K. Mootha, S. Mukherjee, B.L. Ebert, M.A. Gillette, A. Paulovich, S.L. Pomeroy, T.R. Golub, E.S. Lander, and J.P. Mesirov. 2005. Gene set enrichment analysis: a knowledge-based approach for interpreting genome-wide expression profiles. *Proc. Natl. Acad. Sci. USA*. 102:15545–15550. http://dx.doi.org/10.1073/pnas.0506580102

Thol, F., R. Bollin, M. Gehlhaar, C. Walter, M. Dugas, K.J. Suchanek, A. Kirchner, L. Huang, A. Chaturvedi, M. Wichmann, et al. 2014. Mutations in the cohesin complex in acute myeloid leukemia: clinical and prognostic implications. *Blood*. 123:914–920. http://dx.doi.org/10.1182/blood-2013-07-518746

Thota, S., A.D. Viny, H. Makishima, B. Spitzer, T. Radivoyevitch, B. Przychodzen, M.A. Sekeres, R.L. Levine, and J.P. Maciejewski. 2014. Genetic alterations of the cohesin complex genes in myeloid malignancies. *Blood*. 124:1790–1798. http://dx.doi.org/10.1182/blood-2014-04-567057

Welch, J.S., T.J. Ley, D.C. Link, C.A. Miller, D.E. Larson, D.C. Koboldt, L.D. Wartman, T.L. Lamprecht, F. Liu, J. Xia, et al. 2012. The origin and evolution of mutations in acute myeloid leukemia. *Cell*. 150:264–278. http://dx.doi.org/10.1016/j.cell.2012.06.023

Wendt, K.S., K. Yoshida, T. Itoh, M. Bando, B. Koch, E. Schirghuber, S. Tsutsumi, G. Nagae, K. Ishihara, T. Mishiro, et al. 2008. Cohesin mediates transcriptional insulation by CCCTC-binding factor. *Nature*. 451:796–801. http://dx.doi.org/10.1038/nature06634

Whyte, W.A., D.A. Orlando, D. Hnisz, B.J. Abraham, C.Y. Lin, M.H. Kagey, P.B. Rahl, T.I. Lee, and R.A. Young. 2013. Master transcription factors and mediator establish super-enhancers at key cell identity genes. *Cell*. 153:307–319. http://dx.doi.org/10.1016/j.cell.2013.03.035

Wierenga, A.T., E. Vellenga, and J.J. Schuringa. 2008. Maximal STAT5-induced proliferation and self-renewal at intermediate STAT5 activity levels. *Mol. Cell. Biol.* 28:6668–6680. http://dx.doi.org/10.1128/MCB.01025-08

Zhang, S., S. Fukuda, Y. Lee, G. Hangoc, S. Cooper, R. Spolski, W.J. Leonard, and H.E. Broxmeyer. 2000. Essential role of signal transducer and activator of transcription (Stat)5a but not Stat5b for Flt3-dependent signaling. *J. Exp. Med*. 192:719–728.